Laser & Photonics Reviews / Volume 18, Issue 2 / 2300539

Research Article | Full Access

Tunable Optofluidic Curvature for Micromanipulation

Gopal Verma, Gyanendra Yadav, Yuzhi Shi, Lei-Ming Zhou, Cheng-Wei Qiu, Wei Li

First published: 27 November 2023
https://doi.org/10.1002/lpor.202300539

UBC eLink

Abstract

Manipulating micro/nanoparticles on deformed liquid interfaces induced by radiation pressure presents an active, non-invasive, and contactless method. However, a significant challenge arises due to the relatively small magnitude of the radiation force in normal incidence. Nevertheless, this technique holds immense utility in controlling particle movement at interfaces, with numerous applications in both physical and biological contexts. To overcome this, the peculiar properties of total internal reflection (TIR) in retro-reflection mode are expoited to create a $\approx 1\ \mu m$ high amplitude bulge on the water surface, which can migrate $2\ \mu m$ radius particles as forcibly as the traditional micro-post paradigm. The bulge height is measured using an interferometric technique, and the underlying physics are demonstrated using an imitated particle with a capillary charge. By shining two pump lasers, an interface shape is created with increasing complexity, and the relative pump laser intensity is tuned to migrate particles in the desired direction. The method provides a non-invasive and contactless way to remotely actuate almost all types of micro/nanoparticles at the liquid surface.

1 Introduction

Capillary forces are interactions between objects that are mediated by the curved interfaces of fluids.[1-4] These forces arise when objects come into contact with the fluid phase boundary, causing perturbations in the shape of the interface.[1-10] The magnitude of these forces is dependent on the wetting properties[9-11] and surface characteristics of the objects,[8-10, 12-14] and they can affect objects of various sizes, ranging from nanometers to centimeters.[5] Capillary forces have been observed in nature, such as in the meniscus-

climbing technique of insects,[15] and in laboratory experiments.[3] They are also sufficient to drive the self-assembly of micro-sized cylinders on curved liquid interfaces.[3] Thus, curved fluid interfaces hold significant potential for directed particle migration and trapping at the interface,[16-18] and have various technological applications.

Various techniques, including optical tweezers,[19-22] acoustic traps,[23] electro-kinetic traps,[24, 25] magnetic tweezers,[26, 27] light-induced hydrodynamic flows,[28, 29] light-induced elastic waves,[30] and thermocapillary deformation of the liquid interface,[31] have been used for trapping and manipulating dielectric/biological particles. Some methods involve pinning the liquid interface to micro-posts and hydrophobic patches[3, 8] to steer particles along complex trajectories, while others use long-range curvature to study fluid responses to electric, magnetic, or optical fields.[32, 33] However, these methods often require complex experimental setups and have limitations, such as unwanted heating effects due to direct laser interaction with the trapping particle or passive liquid interface pinning that is not easily reconfigurable without changing the micro-post. Additionally, using an electric or magnetic field to trap particles near the liquid interface can cause complications by interacting with the liquid. Therefore, there is a need for simple, tunable, and non-invasive methods to reconfigure the interface and direct micro/nano particles at the liquid surface.

In this article, we employed a pump-probe laser-based approach to generate and measure a tunable surface curvature field at the air-water (AW) interface for manipulating microparticles. We utilized the intriguing momentum transfer effect[34, 35] in the retro-reflection mode at near- TIR, which enhanced the optical momentum transfer approximately sixfold compared to normal incidence (4 W TIR equivalent to 24 W in normal incidence). Using a non-invasive interferometric probe with precision, we measured the bulge height to determine the direction and magnitude of the capillary curvature field. We modeled the bulge as an imitated particle with a capillary charge , and its magnitude can be adjusted by changing the pump laser beam's spot size and power. Remarkably, we demonstrated that the curvature capillary energy of a height bulge was capable of directing radius particles at the AW interface. This effect, of similar magnitude to that produced by a micro-post,[3] requires a comparatively much larger meniscus height ( ). Furthermore, we created a tunable complex curvature field using two pump beams that migrate micro-particles in the desired direction by adjusting the relative intensity of the pump laser beams. This approach can be used to direct any absorbing/transparent micro/nanoparticle at a liquid surface without direct exposure to light. This technique may find applications in microfluidics and optofluidics[19, 36-38] for creating precise and tunable curvature fields for directing micro-particles.

2 Results and Discussion

The schematic of our experimental setup is shown in **Figure 1a**. A spherical glass with a large radius was mounted on a three-axis micro-positioner. Due to the large , the meniscus

effect from its walls does not interfere with that produced by the laser. We placed a large water drop on the glass with a thickness H_0 of about , and the typical diameter of the drop was around . A low-power red laser beam, serving as a probe beam, was incident to the center of the drop quasi-normally from above. Two partial reflections from the AW and water-glass interfaces produced a high-contrast Newton-ring-like fringe pattern on the screen.[35, 39] The fringe pattern was self-calibrating for nanoscale measurements and has been used as a direct measurement of laser-induced deformation of the AW interface.[35, 40, 41] To measure the spatial profile of the AW interface, keeping the pump beam fixed, we scanned the probe beam across the AW interface by translating the mirror M3 (Figure 1a).

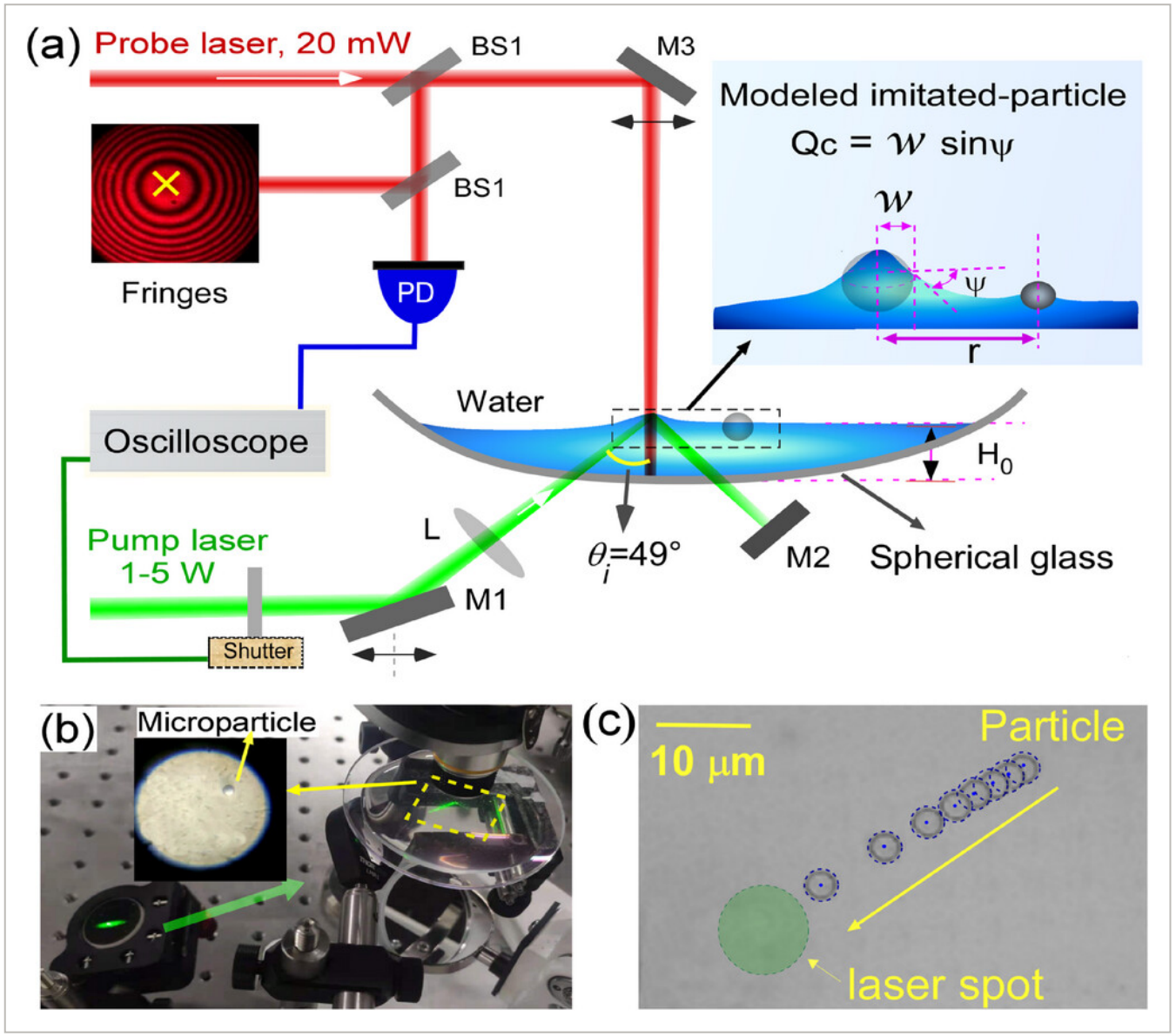

Figure 1

Open in figure viewer | PowerPoint

a) Schematic of the experimental setup. A pump laser beam is used to locally deform the AW interface and the deformation is probed by interferometry with a red He–Ne laser probe. Photo-diode (PD), BS: 50:50 beam splitter,

Mirrors: M1-M3, T = 300 K, and relative humidity of 50%. Inset: Modeled bulge as an imitated particle with the capillary charge (). b) Picture of the set-up. c) Time-stamped image of micro-particle trajectory on an AW interface.

We performed the experiment in retro-path TIR () regime using a mirror M2 to enhance the radiation pressure, hence deformation height times compared to the normal incident. We conducted measurements of the bulge height, as depicted in **Figure** 2a, using two distinct values of the water's surface tension. The reduction in surface tension was achieved by introducing Sodium Dodecyl Sulphate (SDS), following the methodology outlined in reference.[35]

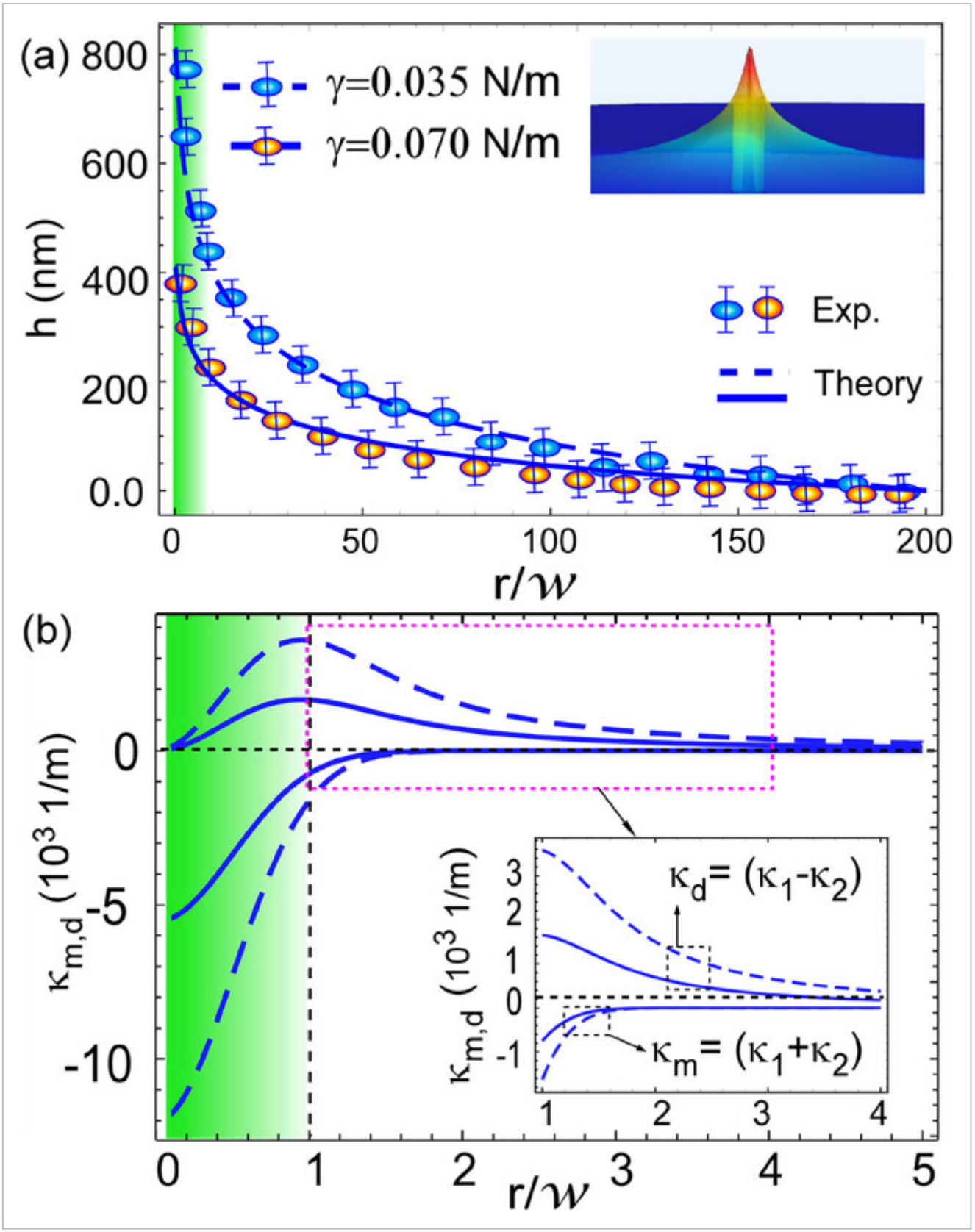

Figure 2

Open in figure viewer | PowerPoint

a) Bulge height of the AW interface for two different surface tension (dashed line) and (solid line) with , . Experimental data (blue and yellow dots) and theory (dashed and solid lines, Equation (2)) are in good agreement. b) Theory plot of versus *r* (for two different surface tension (dashed line) and (solid line)). Inset: their zoom near the beam waist.

2.1 Radiation Pressure Induced Curvature Field

Light momentum discontinuity at the AW interface leads to radiation pressure and can generate a stationary bulge on it. The radiation pressure is balanced by both buoyancy and Laplace pressure at the interface.[35] In the stationary state deformation height of AW interface is given by ref. [35, 36].

(1)

where, c represents the speed of light, P_0 corresponds to the power of the incident light beam, and denotes the refractive index of the liquid (water). The parameter w signifies the waist of the pump laser beam, while and stand for the densities of the liquid and air, respectively. Additionally, γ and g represent the surface tension of the liquid and gravitational acceleration respectively. The spatial dependence is governed by the zeroth-order Bessel function, denoted as J_0. Furthermore, the function is defined as , where and represent the angles of incidence and transmission, respectively. R and T correspond to the reflectance and transmittance at the AW interface, and see Supporting Information details about the force balance equation on the AW interface. This surface has principal curvatures[36] () that depend on position and decrease with distance from the laser beam waist. So that this surface have a mean curvature[36] and deviatoric curvature[42] where, Principal, mean, and deviatoric curvatures are essential concepts in science and engineering, providing key insights into the geometric and mechanical properties of surfaces.[43] Principal curvatures, representing the maximum and minimum curvatures at a point, define local surface shape–informing us whether it is flat, convex, concave, or saddle-shaped. Mean curvature offers the average of principal curvatures, indicating overall surface bending, while deviatoric curvature quantifies variations in curvature across a surface, helping identify regions experiencing uneven deformation or stress. Figure 2a represents the AW bulge height measured by our technique and found good agreement with the theory plot of Equation (2). Furthermore, in Figures S1 and S2 (Supporting Information, we have plotted the power dependence height, curvatures, and Capillary force. To study the interaction of these microparticles with the curved interface, the microparticles are placed on the AW interface. Once attached, the particles are no longer affected by gravity, as the Bond number associated with the particle , which measures the relative magnitude of gravity to the surface. where and a are the density and radius of the particle respectably, g is acceleration due to gravity. The curvature capillary energy E for a particle with a nearly circular cross-section and a pinned contact line trapped on a host interface with arbitrary mean curvature and deviatoric curvature was derived previously.[16] The height of the pinned contact line contour can be decomposed into a multi-pole expansion with the quadrupolar mode of amplitude h_p. The associated curvature capillary energy is ref. [44, 45],

(2)

In this expression, the first term E_0 is independent of the local curvature. The second term predicts that a particle will move to sites of high deviatoric curvature, while the last two terms predict particle migration along gradients of deviatoric and mean curvature. On an interface with spatially varying curvature, the trapping energy changes with position and thus gives rise to a lateral force on the trapped particle. The gradient of the curvature anisotropy pushes the particle toward more strongly curved regions of the interface. We have plotted capillary force using the curvature from Equation (1). Which changes the sign(attractive to repulsive) near the laser beam edge and avoids the particle's direct interaction with the laser. For the given and a, the interface with a steeper curvature gradient, exerts a large capillary force as we found in our photon-momentum-induced bulge of height . It exerts the same order of capillary force due to a steeper curvature gradient (see Figure S2, Supporting Information), as was reported for micro-post and microparticle in refs. [3, 4, 42].

2.2 Experimental Realization of Particle Migration and Capillary Charge

To demonstrate the radiation pressure-induced capillary curvature for micro-particles migration, we prepared a dilute solution of water with polystyrene particles of radius and surface roughness of . We placed a microscope objective (30x) to observe the particle migration, focusing on the water's surface from the top (Figure 1b). We shined a pump laser beam of power and beam waist at the AW interface near the TIR angle. As soon as the laser beam is incident at the AW interface, the particle moves toward the focal spot due to the capillary force. We recorded the video and analyzed it using Tracker software, which gave the particle trajectory as shown in Figure 1c. Details about the force balance of the capillary force and the viscous forces are in (see Supporting Information of force balance section).

Force balance implies , which was confirmed by our experiments (0.23 ± 0.05), as shown in **Figure** 3c. We expect a small discrepancy from 1/4 power law due to the bulge profile around the micro-particle not perfectly quadrupole.[3] Due to repulsive capillary force particle stopped and returned back to the minima of capillary force.

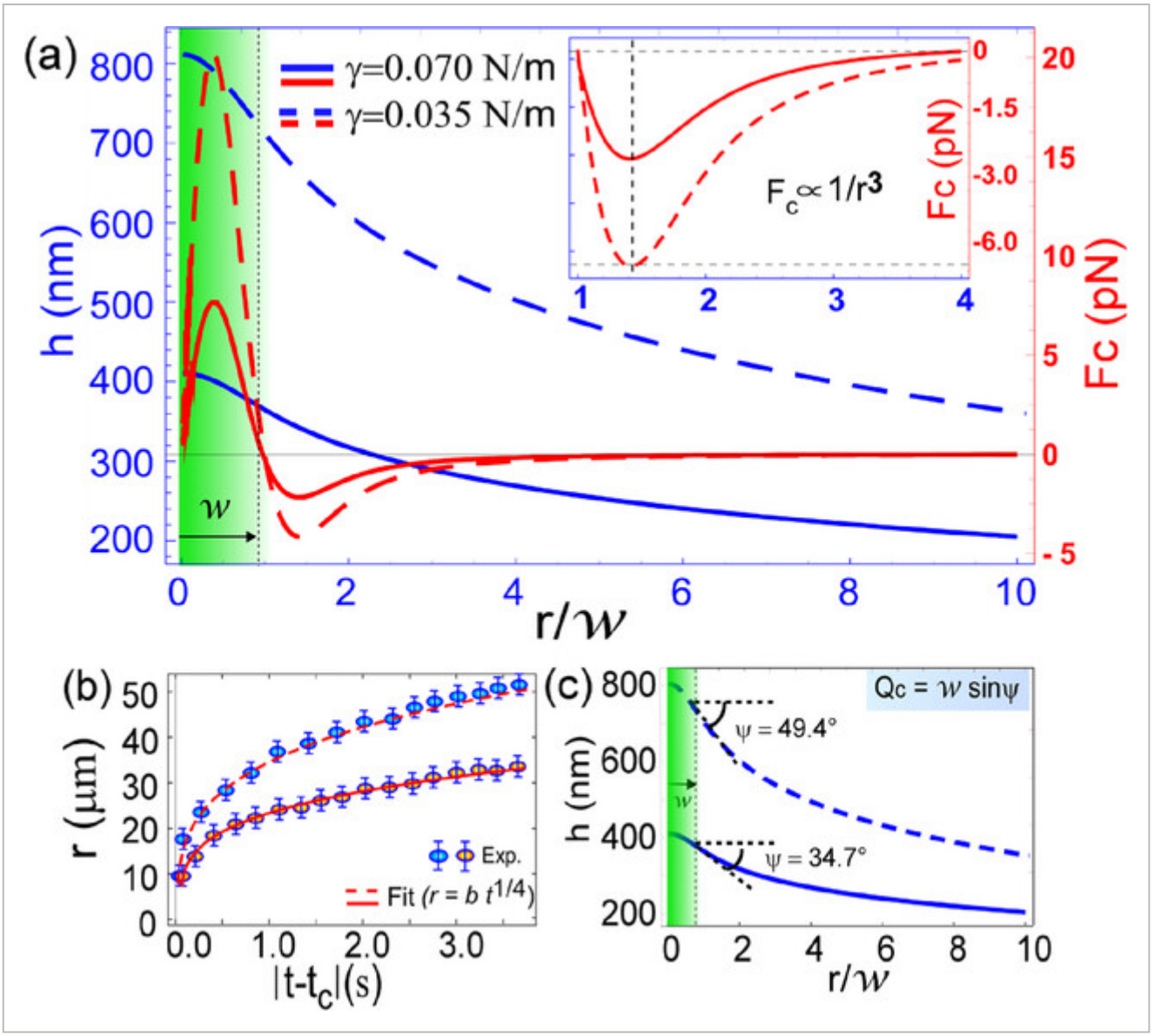

Figure 3

Open in figure viewer | PowerPoint

a) Theoretical plot of *h* versus (Equation (2), left y-axis) and Capillary Force (, right y-axis) for two different surface tensions: (dashed line) and (solid line), with and . b) The radial distance of the migrating microspheres from the center of the laser beam *r*, as a function of time remaining until contact, , where is the time in which the sphere reached the edge of the laser beam c) Capillary charge corresponding to deformed AW interface, which is modeled as an imitated particle (as shown in the inset of Figure 1).

2.3 Optofluidic Bulge as an Imitated Particle with Capillary Charge

As the radiation pressure is balanced by the buoyancy and curvature (see Equation (S1), Supporting Information), their comparison introduces an intrinsic medium-dependent length scale, the capillary length . As deformations are due to the optical momentum of a laser beam of beam waist *w*, we can define an optical bond number as . It means that the induced bulge at the AW interface can be viewed as produced by an imitated particle of

radius *w*.[36, 46] Hence, *w* is a second length scale of optical nature that can be tuned externally and independently to . The interaction of an imitated particle with a real particle is considered an interaction between two capillary charges (), where and ψ are the radius of the triple line and the interfacial angle of a particle and bulge, respectively. One of these represents the real particle, and the second is an imitated particle, as shown in refs. [9, 47]. Although derived initially only for contact angles close to , Velev et al.,[6] have shown that it remains valid even for highly wetting surfaces, and thus for large meniscus slopes in the vicinity of the cylinders. We have calculated the capillary charges created by corresponding to radiation pressure and micropost , as shown in Figure 3c.

Furthermore, in our case as the curvature of the deformed interface follow the power-law , for , the expression for the capillary force between (Monopole and Qudrupole) , which resembles to some extent Coulomb's law of electricity.[7, 9, 47] That is why is called the "capillary charge" of imitated and micro particles. In fact, characterizes the ability of the particle to deform the liquid interface and thus to take part in capillary interactions. Figure 3a shows the bulge height and variation for three *w* and it changes their magnitude and sign near the laser beam edge; hence the particle would repel after this point and avoid trapping at beam focus. This sets a clear difference to the optical tweezers that attract particles to the center of the beam.

2.4 Curvature Field Created By Two Pump Laser Spots

To demonstrate the wide applicability of the technique, we create liquid interface curvature fields of increasing complexity to direct the particle in the desired direction. For this purpose, we designed a set of experiments in which two pump laser beams deform the interface shined near the TIR regime. We directed our pump laser beam at two distinct points situated along the same line, as depicted in **Figure** 4a. Moreover, Figure S3 (Supporting Information) illustrates the deformation of the AW interface profile for two different laser power levels. In Figure 4b,c, we positioned these points in a manner that the principal curvature of the deformed AW interface forms an angle denoted as α (refer to Figure 4d).

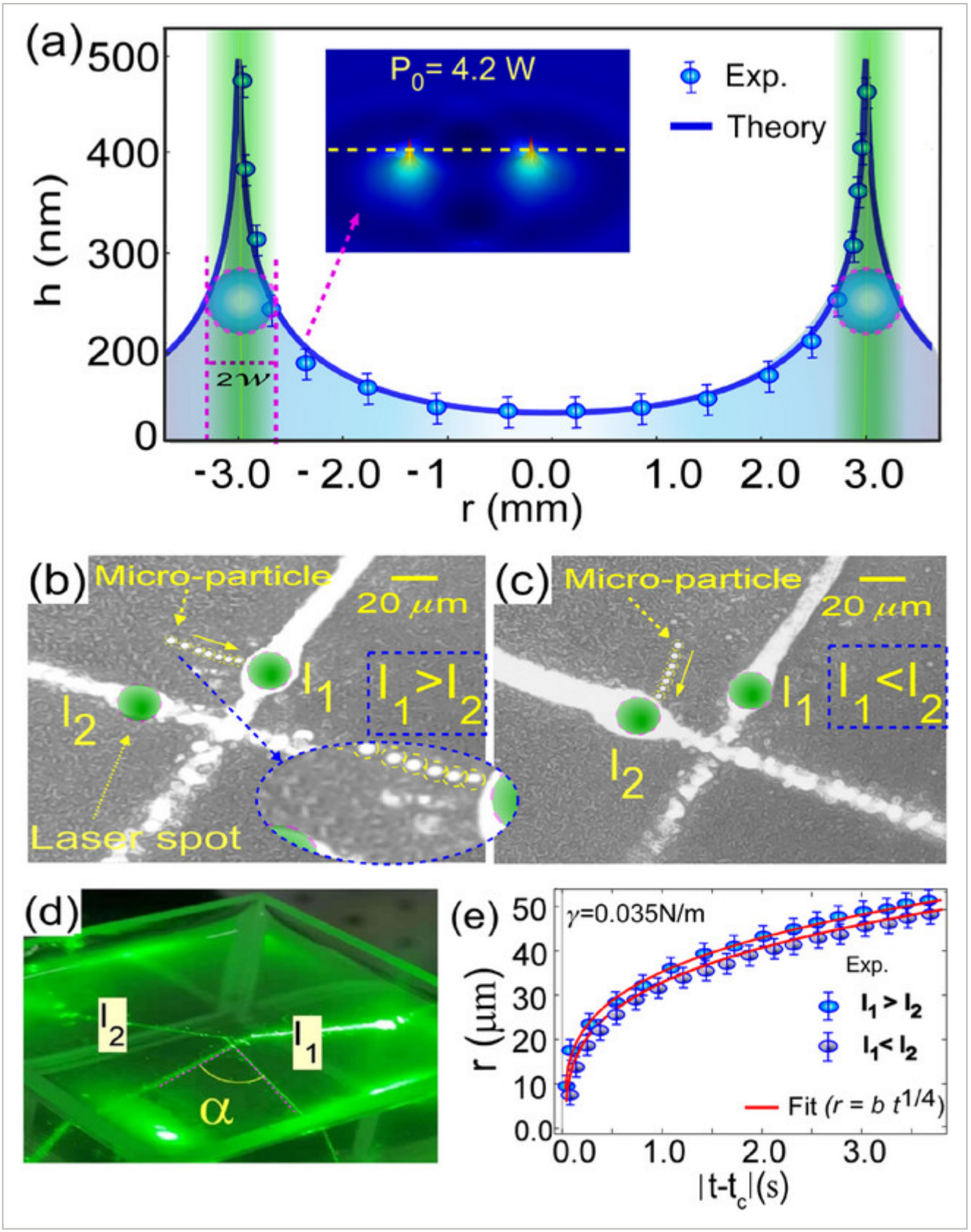

Figure 4

Open in figure viewer | PowerPoint

a) Experimentally measured . Inset: numerically calculated bulge profile. b,c) Time-stamped image of micro-particle trajectory on an AW interface with a laser intensity of . d) Picture of the setup in two-beam configuration. e) Shows the

radial distance *r* of the migrating microspheres from the center of the laser beam, as a function of the time remaining until contact, , where is the time in which the sphere reached the edge of the laser beam.

Consequently, the resulting curvature field direction could induce complex particle trajectories.[3] In addition, for Figure **4b,c**, we conducted micro-particle trajectory recording at two distinct laser intensities denoted as I_1 and I_2. This was achieved by lowering the power of the pump laser while maintaining a constant laser beam waist. Notably, an evident power-law pattern emerged in the particle trajectories, with a power-law fit of observed, as illustrated in Figure **3e**.

Our TIR-enhanced AW deformation strategy offers several potential applications and advantages. First, we modeled the bulge as an imitated particle with a capillary charge, which can be easily tuned by changing the spot size, power, and polarization of the pump laser beam. This is a significant advantage compared to techniques that use micro-posts for micromanipulation,[3] which are limited in their ability to produce complex fluid curvature fields without changing the micro post. Furthermore, using a hollow beam, it is possible to create even more complex fluid curvature fields[48] for more sophisticated micromanipulation. Second, our multiple-beam approach allows for the migration of particles in desired directions by changing the relative intensity of the pump laser beams. This is a powerful tool for precise particle manipulation and has potential applications in microfluidics and optofluidics.[19, 36] Finally, our TIR-enhanced deformation of the AW interface and probing approach provide a means to investigate capillary interactions in the weaker limit, where interactions are closer to thermal excitation . This offers exciting opportunities to explore the fundamental physics of capillary interactions in new regimes, which could have applications in areas such as soft matter physics, biophysics, and materials science.

3 Conclusion

We have realized photon-momentum-induced bulges at the AW interface, which can direct the particle migration in a preferred direction. The tracked trajectories of the microparticles produce strong credibility for our technique's proposal. In a more specific context, this non-contact technique is invaluable for remotely manipulating particles on the liquid's surface, including micro/nanoparticles attached to transparent biological membranes.[49] The approach avoids direct exposure to light, holding substantial promise, especially in biology, and within microfluidics, it enables precise manipulation of micro-objects like cells or beads on the liquid's surface. This new manipulative technique has the capability to generate a significant capillary force without causing any damage. It enhances the potential for broader applications of optical manipulation techniques in fields such as biology and meta-materials.[50, 51] Furthermore, our approach is applicable to particles of various types (including metallic,[52, 53] dielectric, micro/nanoparticles) situated at the liquid surface, with particle sizes ranging from nanometers to centimeters.[5] The only challenge is that heating

effects[54] can outperform radiation pressure-induced deformation. However, it may be overcome by selecting the laser wavelength to avoid the liquid absorption band. Furthermore, it is easily tunable and could be used as a mobile curvature cue to interact with passive microdisks and microspheres on fluid interfaces.[55, 56]

Acknowledgements

This work was supported by the National Natural Science Foundation of China (grant nos. 62134009, 62121005, 12204140) and the Innovation Grant of Changchun Institute of Optics, Fine Mechanics and Physics (CIOMP). The authors gratefully acknowledged the fruitful discussions with Prof. Weiqiang Ding and Dr. Yongyin Cao.

Conflict of Interest

The authors declare no conflict of interest.

Open Research

Data Availability Statement

The data that support the findings of this study are available from the corresponding author upon reasonable request.

Supporting Information

Filename	Description
lpor202300539-sup-0001-SuppMat.pdf 1.7 MB	Supporting Information

Please note: The publisher is not responsible for the content or functionality of any supporting information supplied by the authors. Any queries (other than missing content) should be directed to the corresponding author for the article.

References

1 K. D. Danov, B. Pouligny, P. A. Kralchevsky, *Langmuir* 2001, **17**, 6599.

CAS | Web of Science® | Google Scholar | UBC eLink

2 A. Würger, *Phys. Rev. E* 2006, **74**, 041402.

Google Scholar | UBC eLink

3 M. Cavallaro, L. Botto, E. P. Lewandowski, M. Wang, K. J. Stebe, *Proc Natl. Acad. Sci.* 2011, **108**, 20923.

CAS | PubMed | Web of Science® | Google Scholar | UBC eLink

4 R. Di Leonardo, F. Saglimbeni, G. Ruocco, *Phys. Rev. Lett.* 2008, **100**, 106103.

CAS | PubMed | Web of Science® | Google Scholar | UBC eLink

5 I. Ho, G. Pucci, D. M. Harris, *Phys. Rev. Lett.* 2019, **123**, 254502.

CAS | PubMed | Web of Science® | Google Scholar | UBC eLink

6 O. D. Velev, N. D. Denkov, V. N. Paunov, P. A. Kralchevsky, K. Nagayama, *Langmuir* 1993, **9**, 3702.

CAS | Web of Science® | Google Scholar | UBC eLink

7 C. D. Dushkin, P. A. Kralchevsky, H. Yoshimura, K. Nagayama, *Phys. Rev. Lett.* 1995, **75**, 3454.

CAS | PubMed | Web of Science® | Google Scholar | UBC eLink

8 D. Ershov, J. Sprakel, J. Appel, M. A. Cohen Stuart, J. van der Gucht, *Proc. Natl. Acad.Sci.* 2013, **110**, 9220.

CAS | PubMed | Web of Science® | Google Scholar | UBC eLink

9 P. A. Kralchevsky, K. Nagayama, *Adv. Colloid Interface Sci.* 2000, **85**, 145.

CAS | PubMed | Web of Science® | Google Scholar | UBC eLink

10 P. A. Kralchevsky, K. Nagayama, *Langmuir* 1994, **10**, 23.

CAS | Web of Science® | Google Scholar | UBC eLink

11 A. Domínguez, M. Oettel, S. Dietrich, *J. Chem. Phys.* 2008, **128**, 114904.

PubMed | Google Scholar | UBC eLink

12 W. T. M. Irvine, V. Vitelli, P. M. Chaikin, *Nature* 2010, **468**, 947.

CAS | PubMed | Web of Science® | Google Scholar | UBC eLink

13 J. C. Loudet, A. G. Yodh, B. Pouligny, *Phys. Rev. Lett.* 2006, **97**, 018304.

CAS | PubMed | Web of Science® | Google Scholar | UBC eLink

14 D. Stamou, C. Duschl, D. Johannsmann, *Phys. Rev. E* 2000, **62**, 5263.

CAS | PubMed | Web of Science® | Google Scholar | UBC eLink

15 J. W. M. Hu, D. L. Bush, *Nature* 2005, **437**, 733.

CAS | PubMed | Web of Science® | Google Scholar | UBC eLink

16 C. Blanc, D. Fedorenko, M. Gross, M. In, M. Abkarian, M. A. Gharbi, J.-B. Fournier, P. Galatola, M. Nobili, *Phys. Rev. Lett.* 2013, **111**, 058302.

PubMed | Google Scholar | UBC eLink

17 K. McEnnis, A. D. Dinsmore, T. P. Russell, *Langmuir* 2015, **31**, 5299.

CAS | PubMed | Web of Science® | Google Scholar | UBC eLink

18 M. Sabapathy, V. Kollabattula, M. G. Basavaraj, E. Mani, *Nanoscale* 2015, **7**, 13868.

CAS | PubMed | Web of Science® | Google Scholar | UBC eLink

19 A. A. Kayani, K. Khoshmanesh, S. A. Ward, A. Mitchell, K. Kalantar-zadeh, *Biomicrofluidics* 2012, **6**, 031501.

CAS | PubMed | Web of Science® | Google Scholar | UBC eLink

20 A. Ashkin, J. M. Dziedzic, T. Yamane, *Nature* 1987, **330**, 769.

CAS | PubMed | Web of Science® | Google Scholar | UBC eLink

21 D. Gao, W. Ding, M. Nieto-Vesperinas, X. Ding, M. Rahman, T. Zhang, C. Lim, C.-W. Qiu, *Light: Sci. Appl.* 2017, **6**, e17039.

CAS | PubMed | Web of Science® | Google Scholar | UBC eLink

22 L. Oliveira, W. H. Campos, M. S. Rocha, *Methods and Protoc.* 2018, **1**, 44.

CAS | Google Scholar | UBC eLink

23 X. Ding, S. C. Lin, B. Kiraly, H. Yue, S. Li, I. K. Chiang, J. Shi, S. J. Benkovic, T. J. Huang, *Proc. Natl. Acad. Sci.* 2012, **109**, 11105.

CAS | PubMed | Web of Science® | Google Scholar | UBC eLink

24 A. E. Cohen, W. E. Moerner, *Opt. Express* 2008, **16**, 6941.

CAS | PubMed | Web of Science® | Google Scholar | UBC eLink

25 L. Foret, A. Würger, *Phys. Rev. Lett.* 2004, **92**, 058302.

CAS | PubMed | Web of Science® | Google Scholar | UBC eLink

26 C. Gosse, V. Croquette, *Biophys. J.* 2002, **82**, 3314.

CAS | PubMed | Web of Science® | Google Scholar | UBC eLink

27 N. Vandewalle, L. Clermont, D. Terwagne, S. Dorbolo, E. Mersch, G. Lumay, *Phys. Rev. E* 2012, **85**, 041402.

CAS | Google Scholar | UBC eLink

28 I. D. Stoev, B. Seelbinder, E. Erben, N. Maghelli, M. Kreysing, *eLight* 2021, **1**, 7.

Google Scholar | UBC eLink

29 X. Zhang, B. Gu, C.-W. Qiu, *Light: Sci. Appl.* 2021, **10**, 243.

CAS | PubMed | Google Scholar | UBC eLink

30 W. Lyu, W. Tang, W. Yan, M. Qiu, *Laser Photonics Rev.* 2022, **16**, 2270021.

Google Scholar | UBC eLink

31 A. Karbalaei, R. Kumar, H. J. Cho, *Micromachines* 2016, **7**, 13.

PubMed | Web of Science® | Google Scholar | UBC eLink

32 A. Statsenko, W. Inami, Y. Kawata, *Opt. Commun.* 2017, **402**, 9.

CAS | Web of Science® | Google Scholar | UBC eLink

33 K. Sakai, Y. Yamamoto, *Appl. Phys. Lett.* 2006, **89**, 211911.

Google Scholar | UBC eLink

34 G. Verma, J. Nair, K. P. Singh, *Phys. Rev. Lett.* 2013, **110**, 079401.

PubMed | Google Scholar | UBC eLink

35 G. Verma, K. P. Singh, *Phys. Rev. Lett.* 2015, **115**, 143902.

PubMed | Google Scholar | UBC eLink

36 J. P. Delville, A. Casner, R. Wunenburger, I. Brevik, *Trends in Lasers and Electro-Optics Research*, NovaScience, New York 2006, p. 158.

Google Scholar | UBC eLink

37 A. Minopoli, S. Wagner, E. Erben, W. Liao, I. D. Stoev, E. Lauga, M. Kreysing, *eLight* 2023, **3**, 16.

Google Scholar | UBC eLink

38 Y. Liu, H. Ding, J. Li, X. Lou, M. Yang, Y. Zheng, *eLight* 2022, **2**, 13.

PubMed | Google Scholar | UBC eLink

39 G. Verma, K. P. Singh, *Appl. Phys. Lett.* 2014, **104**, 244106.

Google Scholar | UBC eLink

40 G. Verma, K. Chaudhary, K. P. Singh, *Sci. Rep.* 2017, **7**, 42554.

CAS | PubMed | Google Scholar | UBC eLink

41 G. Verma, H. Chesneau, H. Chraïbi, U. Delabre, R. Wunenburger, J.-P. Delville, *Soft Matter* 2020, **16**, 7904.

CAS | PubMed | Web of Science® | Google Scholar | UBC eLink

42 N. Sharifi-Mood, I. B. Liu, K. J. Stebe, *Soft Matter* 2015, **11**, 6768.

CAS | PubMed | Web of Science® | Google Scholar | UBC eLink

43 M. Umehara, K. Yamada, W. Rossman, *Differential Geometry of Curves and Surfaces*, World Scientific, Singapore 2017.

Google Scholar | UBC eLink

44 P. Galatola, *Soft Matter* 2016, **12**, 328.

CAS | PubMed | Web of Science® | Google Scholar | UBC eLink

45 A. Würger, *Soft Matter* 2016, **12**, 331.

PubMed | Web of Science® | Google Scholar | UBC eLink

46 N. Bertin, H. Chraïbi, R. Wunenburger, J.-P. Delville, E. Brasselet, *Phys. Rev. Lett.* 2012, **109**, 244304.

CAS | PubMed | Google Scholar | UBC eLink

47 I. Legchenkova, G. Chaniel, M. Frenkel, Y. Bormashenko, S. Shoval, E. Bormashenko, *Surf. Innovations* 2018, **6**, 231.

Web of Science® | Google Scholar | UBC eLink

48 G. Verma, G. Yadav, W. Li, *Opt. Lett.* 2023, **48**, 123.

CAS | PubMed | Web of Science® | Google Scholar | UBC eLink

49 I. Koltover, J. O. Rädler, C. R. Safinya, *Phys. Rev. Lett.* 1999, **82**, 1991.

CAS | Web of Science® | Google Scholar | UBC eLink

50 K. J. Stebe, E. Lewandowski, M. Ghosh, *Science* 2009, **325**, 159.

CAS | PubMed | Web of Science® | Google Scholar | UBC eLink

51 Y. Shi, Q. Song, I. Toftul, T. Zhu, Y. Yu, W. Zhu, D. P. Tsai, Y. Kivshar, A. Q. Liu, *Appl. Phys. Rev.* 2022, **9**, 031303.

CAS | Google Scholar | UBC eLink

52 A. B. D. Brown, C. G. Smith, A. R. Rennie, *Phys. Rev. E* 2000, **62**, 951.

CAS | Web of Science® | Google Scholar | UBC eLink

53 Z. Zhan, M. ElKabbash, J. Cheng, J. Zhang, S. Singh, C. Guo, *ACS Appl. Mater. Interfaces* 2019, **11**, 48512.

CAS | PubMed | Web of Science® | Google Scholar | UBC eLink

54 G. Verma, G. Yadav, C. S. Saraj, L. Li, N. Miljkovic, J. P. Delville, W. Li, *Light: Sci. Appl.* 2022, **11**, 115.

CAS | PubMed | Google Scholar | UBC eLink

55 J. M. Rieser, P. E. Arratia, A. G. Yodh, J. P. Gollub, D. J. Durian, *Langmuir* 2015, **31**, 2421.

CAS | PubMed | Web of Science® | Google Scholar | UBC eLink

56 D. Wong, I. B. Liu, E. B. Steager, K. J. Stebe, V. Kumar, *International Conference on Manipulation, Automation and Robotics at Small Scales (MARSS)* 2016, 1.

Google Scholar | UBC eLink